| | |
|---|---|
| **Publication Year** | 2017 |
| **Acceptance in OA** | 2020-09-02T12:52:52Z |
| **Title** | The reflection spectrum of the low-mass X-ray binary 4U 1636-53 |
| **Authors** | Wang, Yanan, Méndez, Mariano, SANNA, ANDREA, Altamirano, Diego, BELLONI, Tomaso Maria Melchiorre |
| **Publisher's version (DOI)** | 10.1093/mnras/stx671 |
| **Handle** | http://hdl.handle.net/20.500.12386/27060 |
| **Journal** | MONTHLY NOTICES OF THE ROYAL ASTRONOMICAL SOCIETY |
| **Volume** | 468 |

Monthly Notices
of the
ROYAL ASTRONOMICAL SOCIETY

MNRAS **468,** 2256–2264 (2017)
Advance Access publication 2017 March 17
doi:10.1093/mnras/stx671

# The reflection spectrum of the low-mass X-ray binary 4U 1636−53

Yanan Wang,[1★] Mariano Méndez,[1] Andrea Sanna,[2] Diego Altamirano[3]
and T. M. Belloni[4]

[1] *Kapteyn Astronomical Institute, University of Groningen, PO BOX 800, NL-9700 AV Groningen, the Netherlands*
[2] *Dipartimento di Fisica, Universitá degli Studi di Cagliari, SP Monserrato-Sestu km 0.7, I-09042 Monserrato, Italy*
[3] *Department of Physics and Astronomy, University of Southampton, Highfield SO17 IBJ, UK*
[4] *Istituto Nazionale di Astrofisica, Osservatorio Astronomico di Brera, Via E. Bianchi 46, I-23807 Merate, Italy*

Accepted 2017 March 15. Received 2017 March 13; in original form 2016 December 23

## ABSTRACT

We present 3–79 keV *NuSTAR* observations of the neutron star low-mass X-ray binary 4U 1636−53 in the soft, transitional and hard state. The spectra display a broad emission line at 5–10 keV. We applied several models to fit this line: A GAUSSIAN line, a relativistically broadened emission line model, KYRLINE, and two models including relativistically smeared and ionized reflection off the accretion disc with different coronal heights, RELXILL and RELXILLLP. All models fit the spectra well; however, the KYRLINE and RELXILL models yield an inclination of the accretion disc of ∼88° with respect to the line of sight, which is at odds with the fact that this source shows no dips or eclipses. The RELXILLLP model, on the other hand, gives a reasonable inclination of ∼56°. We discuss our results for these models in this source and the possible primary source of the hard X-rays.

**Key words:** accretion, accretion discs – X-rays: individual: 4U 1636−53.

## 1 INTRODUCTION

The advent of moderate/high resolution and high effective area X-ray instruments in the last decade has provided numerous examples of reflection spectra in low-mass X-ray binaries (LMXBs; e.g. Cackett et al. 2008) and active galactic nuclei (AGNs; e.g. Parker et al. 2014). The X-ray reflection component produced at the inner edge of the ion disc in these systems is due to fluorescence and Compton scattering (e.g. Guilbert & Rees 1988; Lightman & White 1988; Fabian et al. 1989). The current paradigm is that a power-law component irradiates the surface of the accretion disc and the X-ray photons then interact with the material producing diverse atomic features. In the case of an accreting neutron star (NS), however, the emission from the NS surface/boundary layer can as well irradiate the accretion disc (Popham & Sunyaev 2001). Generally, the reflection spectrum contains a broad emission line in the 6.4–7.0 keV band due to iron, plus a Compton back-scattering hump at ∼10–30 keV (e.g. Miller et al. 2013; Risaliti et al. 2013). Disc reflection spectra may provide a powerful probe of the ion geometry, like the inner radius and inclination of the ion disc (Fabian et al. 1989).

4U 1636−53 is an NS LMXB classified as an atoll source (Hasinger & van der Klis 1989) with an orbital period of ∼3.8 h (van Paradijs et al. 1990) and a companion star of mass ∼0.4 M$_\odot$ (Giles et al. 2002), at a distance of 6 kpc (Galloway et al. 2006). Besides the high variability (e.g. Altamirano et al. 2008; Sanna et al. 2014), a broad and asymmetric emission line probably due to Fe–K has been observed in this system (e.g. Pandel, Kaaret & Corbel 2008; Cackett et al. 2010). Pandel et al. (2008) reported relativistic lines in three *XMM–Newton* observations of 4U 1636−53 and interpreted the line profile as due to the blending of at least two Fe–K lines from iron in different ionization states. Cackett et al. (2010) analysed the spectra of 10 NS LMXBs, including 4U 1636−53, and found that the lines can be fitted equally well by a phenomenological and a reflection model in most cases. In their work, Cackett et al. (2010) employed a reflection model assuming illumination by a blackbody component, implying the boundary layer illuminates a geometrically thin disc.

Ng et al. (2010) analysed the same spectra as Pandel et al. (2008) and Cackett et al. (2010), but found that the lines could be fitted well with a GAUSSIAN model, suggesting a symmetric line profile. Ng et al. (2010) interpreted the line width as the result of broadening due to Compton scattering in the surface layers of the ion disc. The analyses of Pandel et al. (2008) and Ng et al. (2010) differ in some ways. For instance, Ng et al. (2010) took pileup and background effects into account, while Pandel et al. (2008) also fitted the simultaneous *Rossi X-ray Timing Explorer* (*RXTE*) observations and did not correct for pileup in their work, which might also cause the difference of the line profiles because of the different continuum.

Sanna et al. (2013) analysed six *XMM–Newton* observations of 4U 1636−53 with different models, including both symmetric and assymmetric line profiles. They found that in four observations, the

---

★ E-mail: yanan@astro.rug.nl

© 2017 The Authors
Published by Oxford University Press on behalf of the Royal Astronomical Society

Downloaded from https://academic.oup.com/mnras/article-abstract/468/2/2256/3073721 by guest on 20 July 2020

**Table 1.** *NuSTAR* Observations of 4U 1636−53 used in this paper.

| Observation | Identification number | Observation time (UTC) | Exposure (ks) |
|---|---|---|---|
| | | (day.month.year hr:min) | |
| Observation 1 | 30102014002 | 25.08.2015 02:51–25.08.2015 18:36 | $27.4^A$ (27.3*)/$27.7^B$ (27.5*) |
| Observation 2 | 30102014004 | 05.09.2015 17:41–06.09.2015 11:01 | $30.3^A$ (30.2*)/$30.4^B$ (30.3*) |
| Observation 3 | 30102014006 | 18.09.2015 07:06–18.09.2015 23:26 | $28.9^A$ (28.8*)/$29.0^B$ (28.9*) |

*Notes.* $^A$Total exposure time of FPMA of *NuSTAR*;
$^B$Total exposure time of FPMB of *NuSTAR*;
*Final exposure time excluding X-ray bursts.

primary source of the hard X-rays that reflect off the disc was the NS surface/boundary layer, and in two observations, the primary source was the corona.

Additionally, the Fe line profile in 4U 1636−53 shows a blue wing extending to high energies (Pandel et al. 2008), which indicates a high inclination, even though neither eclipses or dips have been observed in this source. Sanna et al. (2013) also reported a high inclination of the source in most cases. Sanna et al. (2013) tried both phenomenological and reflection models, but none of these models helped solving this high-inclination issue.

The *Nuclear Spectroscopic Telescope Array* (*NuSTAR*, Harrison et al. 2013) is the first focusing high energy (3–79 keV) X-ray observatory. Compared with *XMM–Newton*, *NuSTAR* can simultaneously observe the broad emission line and the Compton hump without pileup effects, so it offers an ideal opportunity to study the reflection spectra not only in LMXBs but also in AGN. The good energy resolution and sensitivity of *NuSTAR* allow us to better constrain the hard X-ray continuum, identifying the presence of Comptonization and of a cut-off in the high energy emission. Recently, Ludlam et al. (2017) analysed one *NuSTAR* observation of 4U 1636−53 in the hard state, and they found a high inclination of 76.5°–79.9° for a spin parameter of 0.0–0.3, which is consistent with the inclination derived from the other papers above. Here, we report on another three observations of 4U 1636−53 taken with *NuSTAR*, which are subsequent to the observation in Ludlam et al. (2017), while the source was in different states. We apply different models to investigate the characteristics of the line and compare those characteristics in different states of the source.

## 2 OBSERVATIONS AND DATA REDUCTION

The X-ray data used here consist of three observations with *NuSTAR* taken between 2015 August 25 and September 18. We report the details of the observations in Table 1. We marked the time of the three *NuSTAR* observations presented here in Fig. 1, which shows the publicly available *Swift*/BAT daily-averaged light curve (15–50 keV, top panel)[1] and the MAXI daily-averaged light curve (2–4 keV, lower panel).[2] The light curve of 4U 1636−53 in Fig. 1 shows a ∼35–40 d long-term evolution (Shih et al. 2005; Belloni et al. 2007) related to spectral changes as the system moves between the hard and soft spectral states, which indicates that the source evolves from the soft to the transitional, and the hard state from Observations 1 to 3. In Fig. 1, we also marked the observation analysed by Ludlam et al. (2017), in which, according to these authors, the source was in the hard state.

We processed the *NuSTAR* data using the *NuSTAR* Data Analysis Software (NUSTARDAS) version 1.5.1. (Harrison et al. 2013). We extracted light curves and spectra with the command *nuproducts* using a circular extraction region of 100 arcsec for both focal plane modules A and B (FPMA/B). We used another similar sized region away from the source, avoiding the stray light from a nearby source, as the background spectra. There were seven type I X-ray bursts in total in the three observations. A more detailed discussion of the bursts will be presented in a separated paper. We created good time intervals to eliminate the bursts from the spectra of the persistent emission. Finally, we grouped the spectra with a minimum of 25 counts per spectral bin using the task *grppha* within FTOOLS.

## 3 SPECTRAL ANALYSIS AND RESULTS

We used the spectral analysis package XSPEC version 12.9.0 to fit the *NuSTAR* spectra of 4U 1636−53 between 3 and 79 keV, except for the observation 30102014002. The spectrum of observation 30102014002 is very soft and is background dominated at $E > 30$ keV, resulting in the high-energy data becoming very noisy. We therefore restricted the spectral fits of observation 30102014002 to the energy range of 3–30 keV. All errors are quoted at the $1\sigma$ confidence level unless otherwise specified.

We considered each observation observed by two detectors FPMA and FPMB simultaneously as a group and jointly fitted all the groups. In order to account for flux calibration uncertainties, we included a multiplicative constant in our model. In all groups, we fixed the constant to 1 for FPMA and left it free for FPMB. We included a PHABS component in our model to account for the interstellar absorption along the line of sight to this source. When leaving the parameter $N_{\rm H}$ of this component free, it becomes significantly smaller than previously found in this source. Previous studies of 4U 1636−53 with *XMM–Newton*, which extend down to ∼0.5 keV, have found that $N_{\rm H}$ is about $3 \times 10^{21}$ cm$^{-2}$ (e.g. Pandel et al. 2008). *NuSTAR* data only extend down to 3 keV, and hence we cannot constrain $N_{\rm H}$ from our fits. We therefore fixed the value of $N_{\rm H} = 3.1 \times 10^{21}$ cm$^{-2}$ (Zhang et al. 2017).

Following previous studies of the continuum spectra of 4U 1636−53 (e.g. Ng et al. 2010), we initially used a multicolour disc blackbody component to account for emission from the ion disc (DISKBB in XSPEC, Mitsuda et al. 1984), a single temperature blackbody that represents the emission from the NS surface and the boundary layer (BBODY in XSPEC), and a thermal Comptonization component (NTHCOMP in XSPEC, Zdziarski, Johnson & Magdziarz 1996; Życki, Done & Smith 1999). Compared to an exponentially cut-off power law, the NTHCOMP component offers a sharper high-energy cut-off and a more accurate low-energy rollover with similar parameters. In previous works, using *XMM–Newton*, the temperature of the DISKBB component was kT$_{\rm dbb}$ ∼ 0.2–0.8 keV

---

[1] http://swift.gsfc.nasa.gov/results/transients/4U1636-536/
[2] http://maxi.riken.jp/top/

Downloaded from https://academic.oup.com/mnras/article-abstract/468/2/2256/3073721 by guest on 20 July 2020

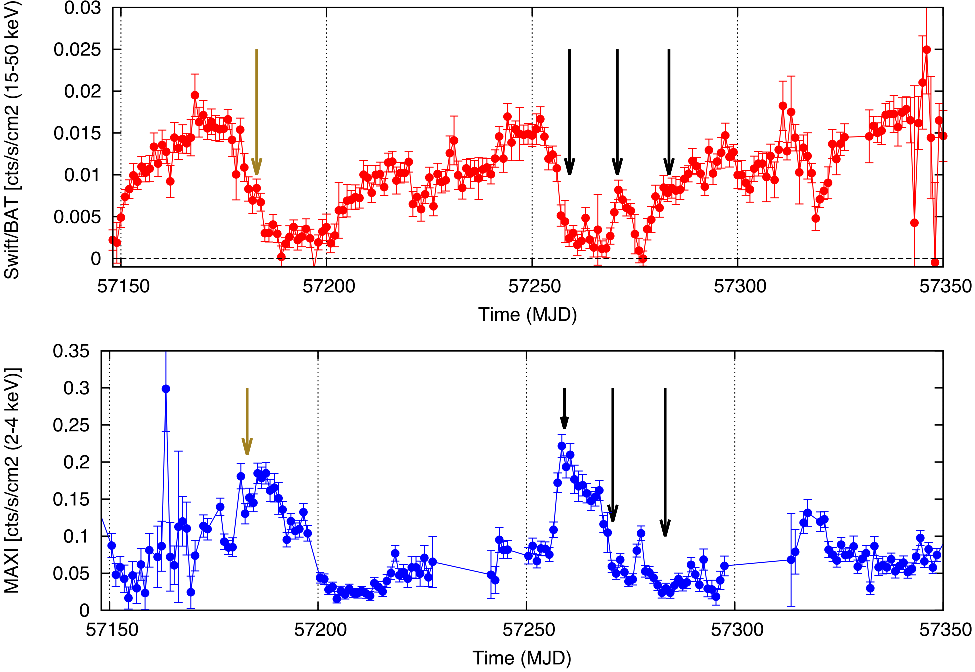

**Figure 1.** Hard and soft long-term light curves of 4U 1636−53. Top and bottom panels show, respectively, the *Swift*/BAT (15–50 keV) and the MAXI (2–4 keV) light curve of this source. The olive and black arrows mark, respectively, the times of the *NuSTAR* observation used in Ludlam et al. (2017) and the three *NuSTAR* observations discussed in this paper.

(e.g. Sanna et al. 2013; Lyu et al. 2014). Given that *NuSTAR* only covers the spectrum above 3 keV, it is not possible to constrain this component with these data. All our fits give equally good results if we exclude the DISKBB component from the model. Therefore, we did not include this component in the rest of the analysis. We note that this does not mean that there is no disc emission in this source (for instance, as we discuss below, the most likely source of the seed photons of the NTHCOMP component is actually the disc); it is only that *NuSTAR* data do not allow us to constrain the direct emission of the disc in this source.

The seed photons in the NTHCOMP component could either come from the DISKBB component or the BBODY component. Sanna et al. (2013) explored the origin of the seed photons by linking the seed photon temperature ($kT_{\rm seed}$) in the NTHCOMP component to either the temperature of the DISKBB component, $kT_{\rm dbb}$, or to that of the BBODY component, $kT_{\rm bb}$, respectively, and they concluded that the seed photons must come from the disc. Given that we have no DISKBB component in our model, we initially set $kT_{\rm seed}$ equal to $kT_{\rm bb}$. The BBODY component in this case became insignificant, similar to what Sanna et al. (2013) found. We therefore left the $kT_{\rm seed}$ in the NTHCOMP component free to vary with a lower limit at 0.01 keV. Following Sunyaev & Titarchuk (1980), the scattering optical depth of the Comptonizing medium, $\tau$, can be calculated from the temperature of the Comptonizing electrons, $kT_{\rm e}$, and the power-law photon index, $\Gamma$, as

$$\tau = \sqrt{2.25 + \frac{3}{(kT_{\rm e}/511\,{\rm keV})[(\Gamma+0.5)^2 - 2.25]}} - 1.5. \qquad (1)$$

After fitting the data with a model containing these components, we still found large positive residuals around 5–10 keV (see Fig. 2), which suggests a possible emission line from Fe–K here. In order to check whether these residuals were due to the continuum model

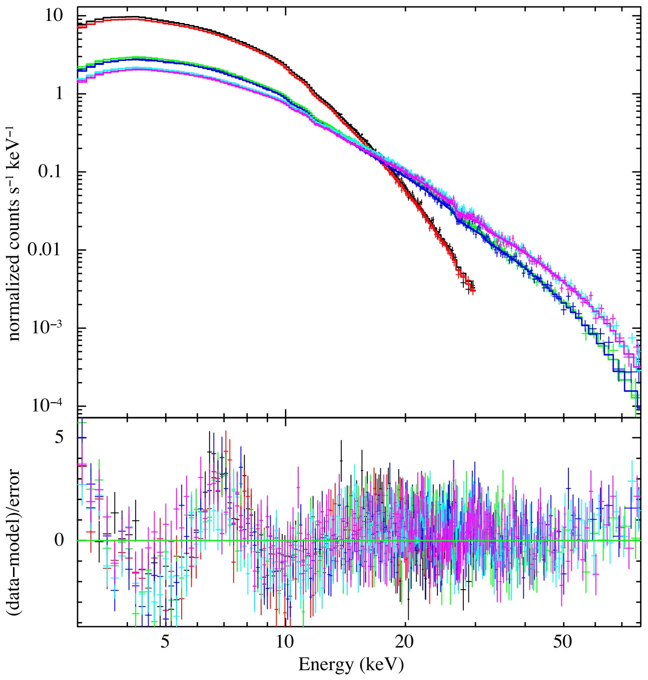

**Figure 2.** *NuSTAR* spectra and models for the fit with CONST*PHABS*(BBODY+NTHCOMP) for 4U 1636−53. The black, red, green, blue, light blue and magenta lines in the top panel represent each spectrum (FPMA/B) listed from top to bottom in Table 1, separately. The bottom panel shows the residuals in terms of sigmas; the colours are the same as in the top panel. The spectra have been rebinned for plotting purposes.

Downloaded from https://academic.oup.com/mnras/article-abstract/468/2/2256/3073721 by guest on 20 July 2020

**Table 2.** Best-fitting parameters of the *NuSTAR* spectra of 4U 1636−53 with Model 1.

| | Component | Model 1<br>Observation 1 | <br>Observation 2 | <br>Observation 3 |
|---|---|---|---|---|
| | constant | $1.00^f/1.02 \pm 0.01$ | | |
| BB | $kT_{\rm bb}$ (keV) | $2.03 \pm 0.02$ | $1.51 \pm 0.07$ | $0.88 \pm 0.02$ |
| | $k_{\rm bb}$ ($10^{-3}$) | $5.9 \pm 0.2$ | $0.3 \pm 0.1$ | $0.8 \pm 0.1$ |
| | $F_{\rm bb}$ ($10^{-11}$) | $45.5 \pm 0.8$ | $2.3 \pm 0.3$ | $3.2 \pm 0.1$ |
| | | $44.5 \pm 1.0$ | $2.1 \pm 0.3$ | $3.6 \pm 0.1$ |
| GAUSSIAN | $E_{\rm gau}$ (keV) | $6.72 \pm 0.06$ | $6.40^{+0.03}_{-0p}$ | $6.40^{+0.03}_{-0p}$ |
| | $\sigma$ (keV) | $1.23 \pm 0.10$ | $1.35 \pm 0.05$ | $1.22 \pm 0.06$ |
| | $k_{\rm gau}$($10^{-3}$) | $3.0 \pm 0.3$ | $2.3 \pm 0.2$ | $1.1 \pm 0.1$ |
| | EW(keV) | $0.17 \pm 0.03$ | $0.33^{+0.10}_{-0.04}$ | $0.27 \pm 0.09$ |
| | | $0.17 \pm 0.03$ | $0.71^{+0.05}_{-0.10}$ | $0.24 \pm 0.07$ |
| | $F_{\rm gau}$ ($10^{-11}$) | $3.25 \pm 0.23$ | $2.26 \pm 0.09$ | $1.02 \pm 0.10$ |
| | | $3.30 \pm 0.25$ | $2.40 \pm 0.09$ | $1.38 \pm 0.06$ |
| NTHCOMP | $\Gamma_{\rm nth}$ | $2.33 \pm 0.02$ | $2.04 \pm 0.01$ | $1.79 \pm 0.01$ |
| | $kT_{\rm e}$(keV) | $3.7 \pm 0.04$ | $16.9 \pm 0.5$ | $20.9 \pm 0.7$ |
| | $\tau$ | $7.5 \pm 0.3$ | $3.4 \pm 0.1$ | $3.7 \pm 0.2$ |
| | $kT_{\rm seed}$(keV) | $0.13^{+0.10}_{-0.13}$ | $0.25^{+0.05}_{-0.24}$ | $0.06^{+0.32}_{-0.06}$ |
| | $k_{\rm nth}$ | $1.36 \pm 0.08$ | $0.25 \pm 0.03$ | $0.12 \pm 0.06$ |
| | $F_{\rm nth}$ ($10^{-9}$) | $1.64 \pm 0.01$ | $1.07 \pm 0.01$ | $1.12 \pm 0.01$ |
| | | $1.63 \pm 0.01$ | $1.07 \pm 0.01$ | $1.13 \pm 0.01$ |
| | Total flux $F_{\rm ttl}$ ($10^{-9}$) | $2.12 \pm 0.01$ | $1.12 \pm 0.01$ | $1.16 \pm 0.01$ |
| | | $2.12 \pm 0.01$ | $1.12 \pm 0.01$ | $1.18 \pm 0.01$ |
| | $\chi^2_\upsilon$ (dof) | 1.04(4637) | | |

*Notes.* $k_{\rm bb}$, $k_{\rm gau}$ and $k_{\rm nth}$ are the normalization of each component in units of photonskeV$^{-1}$ cm$^{-2}$ s$^{-1}$. All the flux as $F_{\rm bb}$, $F_{\rm gau}$, $F_{\rm nth}$ and $F_{\rm ttl}$, represent the unabsorbed flux in units of erg cm$^{-2}$ s$^{-1}$ in the 3–79 keV range. The symbol, $p$, indicates that the energy of the GAUSSIAN component pegged at the lower limit. Errors are quoted at 1$\sigma$ confidence level.

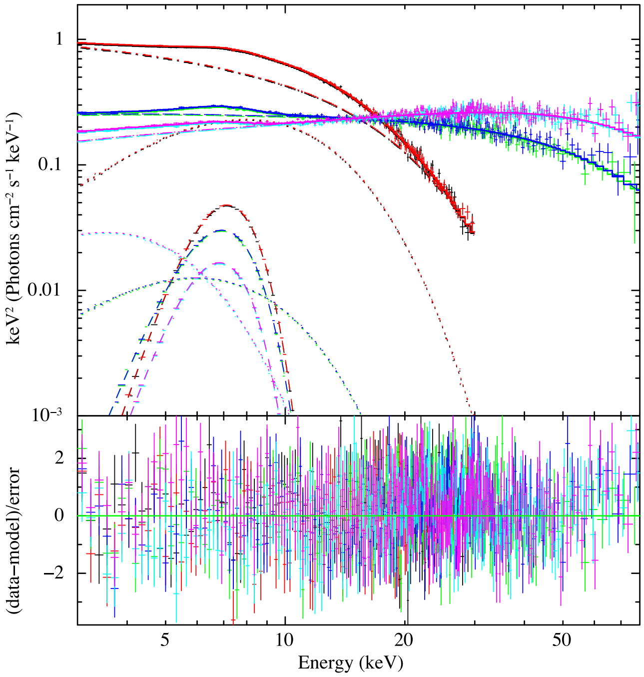

**Figure 3.** *NuSTAR* unfolded spectra and models fitted with the model CONST*PHABS*(BBODY+GAUSSIAN+NTHCOMP) for 4U 1636−53. The colours are the same as in Fig. 2. The dot, dash and dash–dotted lines represent the BBODY, GAUSSIAN and NTHCOMPT components in our model, respectively. Notice that in the top panel of the following spectra figures, the $y$-axis always shows $E^2f(E)$. The bottom panel shows the residuals in terms of sigmas. The best-fitting parameters are given in Table 2.

we used, we replaced the NTHCOMP component by a simple power-law component with a high-energy exponential roll-off (CUTOFFPL in XSPEC). We got similar positive residuals in this case as well.

To try and fit these residuals, we first added a simple Gaussian component to the model. We constrained the energy of the GAUSSIAN component to be between 6.4 and 7 keV, and left the width ($\sigma$) and normalization ($k_{\rm gau}$) free. The entire model we used was CONST*PHABS*(BBODY+GAUSSIAN+NTHCOMP), hereafter, Model 1. For every component, we linked all the free parameters within each observation. The best-fitting parameters of Model 1 are listed in Table 2; the corresponding spectra, individual components and residuals are shown in Fig. 3.

In all three observations, the temperature of the seed photons, $kT_{\rm seed}$, in the NTHCOMP component is not well constrained and is consistent with zero. The power-law photon index, $\Gamma_{\rm nth}$, of the NTHCOMP component decreases while the cut-off energy, $kT_{\rm e}$, increases from Observations 1 to 3. The optical depth, $\tau$, drops abruptly from Observations 1 to 2 and then remains more or less constant from Observations 2 to 3. Based on previous spectral analyses of 4U 1636−53 (e.g. Sanna et al. 2013), the trend of these parameters implies that the Observations 1, 2 and 3 sampled the source, respectively, in the soft, the transitional and the hard state. The energy of the GAUSSIAN component, $E_{\rm gau}$, decreases from ∼6.7 keV in Observation 1 to ∼6.4 keV in Observations 2 and 3, which means that the disc becomes less ionized. If we allowed the energy of the line to be below 6.4 keV (in our case we constrained it to be between 5 and 7 keV) because of a possible gravitational redshift, we found that the energy of the line in Observation 1 does not change significantly, in this case being $6.72 \pm 0.1$ keV with $\sigma = 1.23 \pm 0.20$, but the energy of the line in Observations 2 and 3 decreases to $6.17 \pm 0.13$ keV with $\sigma = 1.56 \pm 0.12$ and $5.35^{+0.55}_{-0.43}$ keV with $\sigma = 1.75 \pm 0.23$, respectively. The $kT_{\rm bb}$ goes down with time. The flux of the GAUSSIAN component, $F_{\rm gau}$, decreases all the time, whereas the fluxes of the BBODY and of the NTHCOMP components decrease at the beginning and slightly increase in the last observation. It is apparent that the emission in the 3–79 keV range is always dominated by the NTHCOMP component. Although the fits with a Gaussian line are statistically acceptable, given the broad profile of the GAUSSIAN ($\sigma$ between 1.2 and 1.5 keV), we also modelled our data with reflection models that include relativistic effects that affect the profile of the line.

### 3.1 Phenomenological reflection model of the line

Compared with the other popular relativistic iron line models (e.g. DISKLINE, LOAR), KYRLINE (Dovčiak, Karas & Yaqoob 2004) allows us to set the spin parameter, $a$, to values different from 0 and 1, and takes the effect of limb darkening in the disc into account. The fit parameters of the model KYRLINE are the dimensionless spin of the NS, $a$, the inclination of the disc, $i_{\rm kyr}$, the inner and outer radii of the disc, $R_{\rm in}$ and $R_{\rm out}$, respectively, the rest energy of the line, $E_{\rm kyr}$, the inner and outer emissivity index, $\alpha$ and $\beta$, respectively, and the normalization of the line, $k_{\rm kyr}$. Assuming that the line is due to iron, from neutral to highly ionized, we constrained $E_{\rm kry}$ to be between 6.4 and 7 keV. Following Braje, Romani & Rauch (2000), the spin parameter is $a = 0.47/P$ (ms), which, for an NS spin of 581 Hz (Zhang et al. 1997; Strohmayer & Markwardt 2002), gives $a = 0.27$, and the smallest possible value for the inner radius

Downloaded from https://academic.oup.com/mnras/article-abstract/468/2/2256/3073721 by guest on 20 July 2020

**Table 3.** Best-fitting parameters of the *NuSTAR* spectra of 4U 1636−53 with Model 2.

| | Component | Model 2 | | |
|---|---|---|---|---|
| | | Observation 1 | Observation 2 | Obs.ervation 3 |
| | constant | $1.00^f/1.02 \pm 0.01$ | | |
| BB | $kT_{\rm bb}$ (keV) | $2.01 \pm 0.01$ | $1.50 \pm 0.04$ | $0.94 \pm 0.03$ |
| | $k_{\rm bb}$ ($10^{-3}$) | $6.1 \pm 0.2$ | $0.6 \pm 0.1$ | $0.8 \pm 0.1$ |
| | $F_{\rm bb}$ ($10^{-11}$) | $46.8 \pm 0.6$ | $4.3 \pm 0.2$ | $3.3 \pm 0.1$ |
| | | $45.9 \pm 0.6$ | $4.1 \pm 0.2$ | $3.8 \pm 0.1$ |
| KYRLINE | $i_{\rm kyr}$ (°) | | $87.6 \pm 0.8$ | |
| | $R_{\rm in}/R_{\rm g}$ | $5.12^{+0.15}_{-0p}$ | $5.12^{+0.10}_{-0p}$ | $5.12^{+0.08}_{-0p}$ |
| | $\alpha = \beta$ | $2.36 \pm 0.11$ | $2.43^{+0.14}_{-0.09}$ | $2.35^{+0.17}_{-0.09}$ |
| | $E_{\rm kyr}$ (keV) | $6.61 \pm 0.06$ | $6.41^{+0.07}_{-0p}$ | $6.40^{+0.04}_{-0p}$ |
| | $k_{\rm kyr}$($10^{-3}$) | $2.73 \pm 0.13$ | $1.55 \pm 0.13$ | $0.89 \pm 0.19$ |
| | EW$_{\rm kyr}$(keV) | $0.15 \pm 0.01$ | $0.24 \pm 0.03$ | $0.18 \pm 0.03$ |
| | | $0.15 \pm 0.01$ | $0.25 \pm 0.03$ | $0.21 \pm 0.01$ |
| | $F_{\rm kyr}$ ($10^{-11}$) | $2.91 \pm 0.11$ | $1.55 \pm 0.05$ | $0.76 \pm 0.05$ |
| | | $2.93 \pm 0.11$ | $1.67 \pm 0.06$ | $1.08 \pm 0.05$ |
| NTHCOMP | $\Gamma_{\rm nth}$ | $2.33 \pm 0.02$ | $2.03 \pm 0.01$ | $1.79 \pm 0.01$ |
| | $kT_{\rm e}$(keV) | $3.8 \pm 0.1$ | $16.5 \pm 0.5$ | $21.1 \pm 0.8$ |
| | $\tau$ | $7.0 \pm 0.2$ | $3.5 \pm 0.2$ | $3.6 \pm 0.2$ |
| | $kT_{\rm seed}$(keV) | $0.14^{+0.15}_{-0.14}$ | $0.14^{+0.17}_{-0.14}$ | $0.15^{+0.20}_{-0.15}$ |
| | $k_{\rm nth}$ | $1.35^{+0.04}_{-0.18}$ | $0.26 \pm 0.01$ | $0.12^{+0.01}_{-0.01}$ |
| | $F_{\rm nth}$ ($10^{-9}$) | $1.63 \pm 0.01$ | $1.06 \pm 0.01$ | $1.12 \pm 0.01$ |
| | | $1.62 \pm 0.01$ | $1.06 \pm 0.01$ | $1.13 \pm 0.01$ |
| | Total flux $F_{\rm ttl}$ ($10^{-9}$) | $2.12 \pm 0.01$ | $1.12 \pm 0.01$ | $1.16 \pm 0.01$ |
| | | $2.12 \pm 0.01$ | $1.12 \pm 0.01$ | $1.18 \pm 0.01$ |
| | $\chi^2_\nu$ (dof) | 1.04(4633) | | |

*Notes.* Units are the same as in Table 2. Errors are quoted at 1$\sigma$ confidence level. The inclination of the KYRLINE component is linked across the three observations.

of the disc is $R_{\rm in} = 5.12R_{\rm g}$, where $R_{\rm g} = GM/c^2$ (Miller, Lamb & Cook 1998). We fixed $R_{\rm out}$ to 400 $R_{\rm g}$. We tied $\alpha$ and $\beta$ to get a single emissivity index. We also included an NTHCOMP component to fit the hard emission of our spectra. Hereafter, we call Model 2 to the model CONST*PHABS*(BBODY+KYRLINE+NTHCOMP). The best-fitting parameters of Model 2 are given in Table 3; the corresponding spectra, individual components and residuals are shown in Fig. 4.

Comparing Tables 2 and 3, we see that all the parameters of the continuum components are more or less the same when we fit the line with either GAUSSIAN or KYRLINE. Only the flux and the equivalent width (EW) of KYRLINE are smaller than those of GAUSSIAN. Even though there are less degrees of freedom in Model 2 than in Model 1, the fit does not improve significantly using KYRLINE compared to GAUSSIAN. Also, as in the case of Model 2 in all observations, $kT_{\rm seed}$ of the NTHCOMP component is not well constrained and is consistent with zero. In all observations, the inner disc radius pegs at the lower limit of the model, and the emissivity index remains more or less constant in all three observations. Remarkably, the inclination is quite high, larger than 80°. The top panel in Fig. 5 shows the $\Delta\chi^2$ of the fit versus the inclination for Model 2.

In addition, the flux or the EW of the KYRLINE component and the flux of the NTHCOMP in Model 2 are anti-correlated. Lyu et al. (2014) found a similar result in their work, in which they used five observations from *Suzaku* and six observations from *XMM–Newton/RXTE*. The best-fitting parameters of the BBODY and NTHCOMP components in Model 1 and 2 here are consistent with the best-fitting parameters of those same components in Lyu et al. (2014) when they fitted

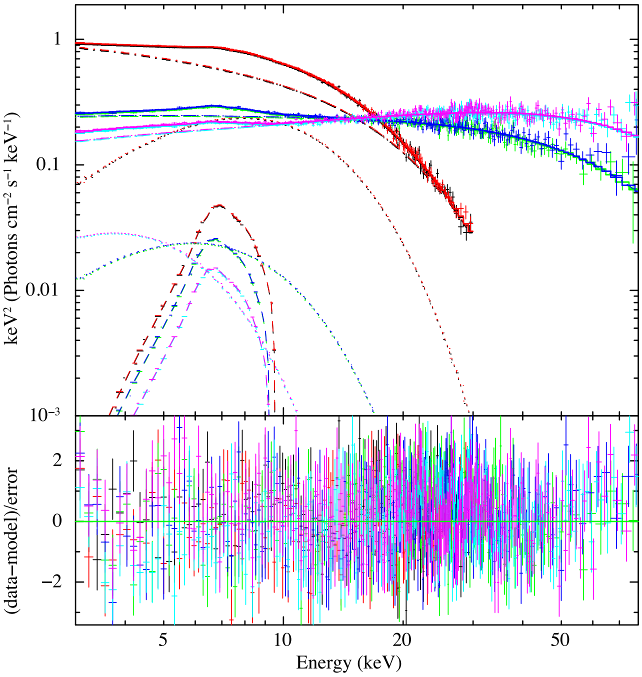

**Figure 4.** *NuSTAR* unfolded spectra and models fitted with the model CONST*PHABS*(BBODY+KYRLINE+NTHCOMP) for 4U 1636−53. Colours and lines are the same as in Fig. 2, except for the dash–dotted line representing the KYRLINE component in this model. The bottom panel shows the residuals in terms of sigmas. The corresponding parameters are given in Table 3.

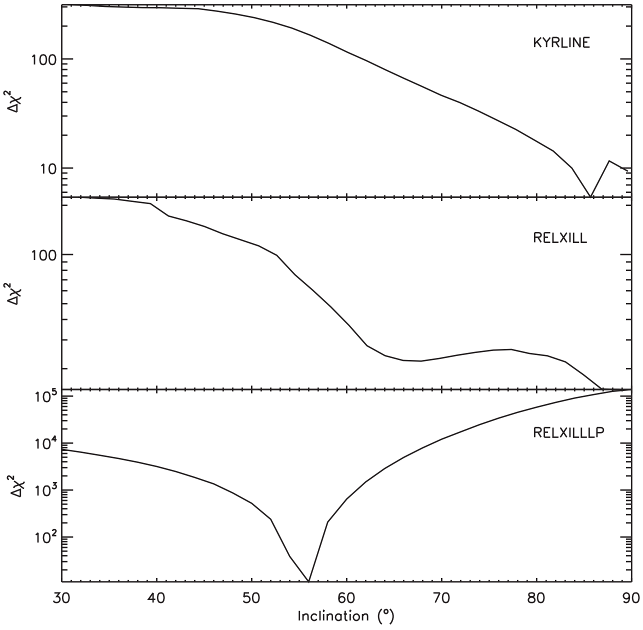

**Figure 5.** The change in the goodness of fit, $\Delta\chi^2$, versus the inclination of different models for the *NuSTAR* observations of 4U 1636−53. The $\Delta\chi^2$ was calculated using the command *steppar* in XSPEC over 30 steps in the inclination angle. The *y*-axis is in logarithmic scale. The panels from top to bottom correspond to the best fitting of Models 1 to 3, respectively.

Downloaded from https://academic.oup.com/mnras/article-abstract/468/2/2256/3073721 by guest on 20 July 2020

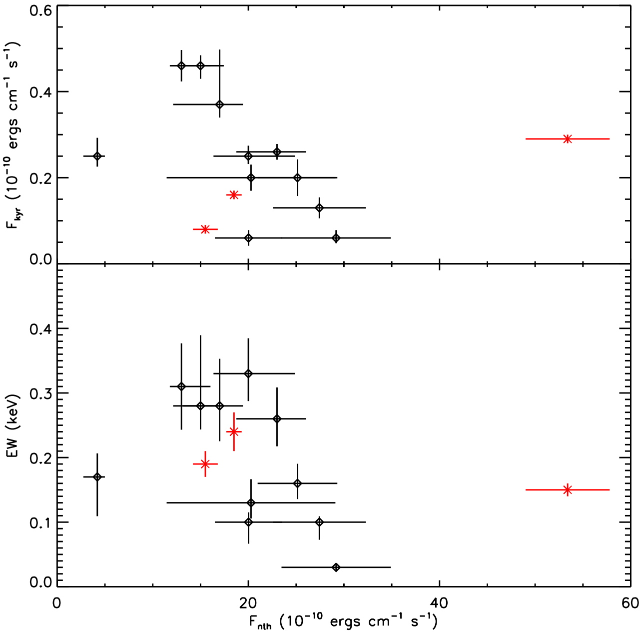

**Figure 6.** The flux (top panel) and EW (bottom panel) of the KYRLINE component versus the flux (0.5–130 keV) of the NTHCOMP component in Model 2 of 4U 1636−53. The three red crosses show the data obtained from *NuSTAR* observations in this work; the 11 back diamonds represent the *Suzaku* and *XMM–Newton/RXTE* data that given by Lyu et al. (2014). Error bars correspond to the 1$\sigma$ uncertainty.

similar models to *XMM–Newton* and *RXTE* data of this source. In Fig. 6, we plot the flux and EW of the KYRLINE component versus the flux of the NTHCOMP component.

### 3.2 Full reflection models

Even though there is no clear reflection hump at high energies (above 10 keV) in the residuals of Fig. 2, the presence of a broad iron line suggests that reflection off the ion disc is important. We therefore fitted the self-consistent relativistic reflection model RELXILL (Dauser et al. 2013, 2016), which describes not only the reflection part, but also a direct power-law component. However, the power-law continuum within RELXILL differs from that in NTHCOMP. In particular, the high-energy cut-off in these two models behaves differently (García et al. 2015). The parameters in this model are the inclination of the disc, $i_{\rm rel}$, the inner and outer radii of the disc, $R_{\rm in}$ and $R_{\rm out}$, respectively, the inner and outer emissivity indexes, $q_{\rm in}$ and $q_{\rm out}$, respectively, the break radius, $R_{\rm break}$, between the two emissivity laws, the spin parameter, $a$, the redshift to the source, $z$, which we fixed to 0, the photon index of the power law, $\Gamma$, the cut-off energy of the power law, $E_{\rm cut}$, the ionization parameter, $\xi$, the iron abundance, $A_{\rm Fe}$, which we fixed to solar, the reflection fraction, $f_{\rm refl}$, and the normalization, $k_{\rm rel}$. The overall model becomes CONST*PHABS*(BBODY+RELXILL), hereafter Model 3. As for KYRLINE, we fixed $a$ to 0.27, and hence $R_{\rm in}$ was forced to be larger than 5.12 $R_{\rm g}$. $R_{\rm out}$ was fixed at 400 $R_{\rm g}$, and $q_{\rm in}$ and $q_{\rm out}$ were linked to vary together. The best-fitting parameters of Model 3 are given in Table 4; the corresponding spectra, individual components and residuals are shown in Fig. 7.

Most of the parameters of Model 3 follow the same trend as those of the other models. The inclination, $i_{\rm rel}$, in Model 3 is still extremely high, consistent with $i_{\rm kyr}$ in Model 2. The inner radius of the disc, $R_{\rm in}$, and cut-off energy, $E_{\rm cut}$, of each observation in Model 3, however,

**Table 4.** Best-fitting parameters of the *NuSTAR* spectra of 4U 1636−53 with Model 3.

| | Component | Model 3 Observation 1 | Observation 2 | Observation 3 |
|---|---|---|---|---|
| | constant | | $1.00^f/1.02 \pm 0.01$ | |
| BB | $kT_{\rm bb}$ (keV) | $2.19 \pm 0.02$ | $1.85 \pm 0.10$ | $0.93 \pm 0.04$ |
| | $k_{\rm bb}$ ($10^{-3}$) | $8.4 \pm 0.1$ | $0.6 \pm 0.1$ | $0.5 \pm 0.1$ |
| | $F_{\rm bb}$ ($10^{-11}$) | $65.8 \pm 0.6$ | $4.5 \pm 0.2$ | $2.2 \pm 0.3$ |
| | | $64.6 \pm 0.5$ | $4.3 \pm 0.3$ | $2.6 \pm 0.3$ |
| RELXILL | $i_{\rm rel}$(°) | | $88.0 \pm 0.3$ | |
| | $R_{\rm in}/R_{\rm g}$ | $5.8 \pm 0.7$ | $16.1^{+4.3}_{-2.7}$ | $16.3^{+15.8}_{-4.5}$ |
| | $q_{\rm in} = q_{\rm out}$ | $2.2 \pm 0.2$ | $5.0^{+4.9}_{-1.4}$ | $4.0^{+2.7}_{-1.0}$ |
| | $\Gamma_{\rm rel}$ | $2.01 \pm 0.05$ | $1.97 \pm 0.02$ | $1.78 \pm 0.04$ |
| | $E_{\rm cut}$ (keV) | $6.5^{+0.4}_{-1.2}$ | $62.8^{+4.4}_{-3.8}$ | $136.0^{+28.8}_{-21.7}$ |
| | $\tau$ | $6.3 \pm 0.9$ | $1.4 \pm 0.1$ | $1.0 \pm 0.2$ |
| | $log(\xi)$ | $3.3 \pm 0.3$ | $3.1 \pm 0.1$ | $2.9 \pm 0.1$ |
| | $refl\_frac$ | $0.9 \pm 0.1$ | $1.7 \pm 0.1$ | $1.2 \pm 0.1$ |
| | $k_{\rm rel}$($10^{-3}$) | $8.6 \pm 0.5$ | $2.5 \pm 0.1$ | $2.3 \pm 0.1$ |
| | $F_{\rm rel}$ ($10^{-9}$) | $1.5 \pm 0.01$ | $1.1 \pm 0.01$ | $1.1 \pm 0.01$ |
| | | $1.5 \pm 0.01$ | $1.1 \pm 0.01$ | $1.2 \pm 0.01$ |
| | Total flux $F_{\rm ttl}$ ($10^{-9}$) | $2.12 \pm 0.01$ | $1.13 \pm 0.01$ | $1.17 \pm 0.01$ |
| | | $2.11 \pm 0.01$ | $1.12 \pm 0.01$ | $1.19 \pm 0.01$ |
| | $\chi^2_v$ (dof) | | 1.03(4636) | |

*Notes.* Units are the same as in Table 2. Errors are quoted at 1$\sigma$ confidence level. The inclination of the RELXILL component is linked across the three observations.

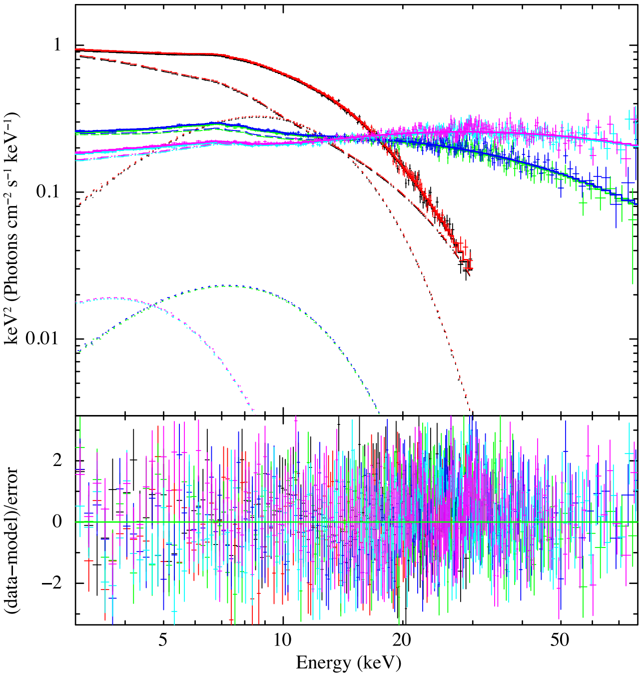

**Figure 7.** *NuSTAR* unfolded spectra and models fitted with the model CONST*PHABS*(BBODY+RELXILL) for 4U 1636−53. Colours are the same in Fig. 2, The dot and dash–dotted line represent the BBODY and RELXILL components in this model. The bottom panel shows the residuals in terms of sigmas. The corresponding parameters are given in Table 4.

Downloaded from https://academic.oup.com/mnras/article-abstract/468/2/2256/3073721 by guest on 20 July 2020

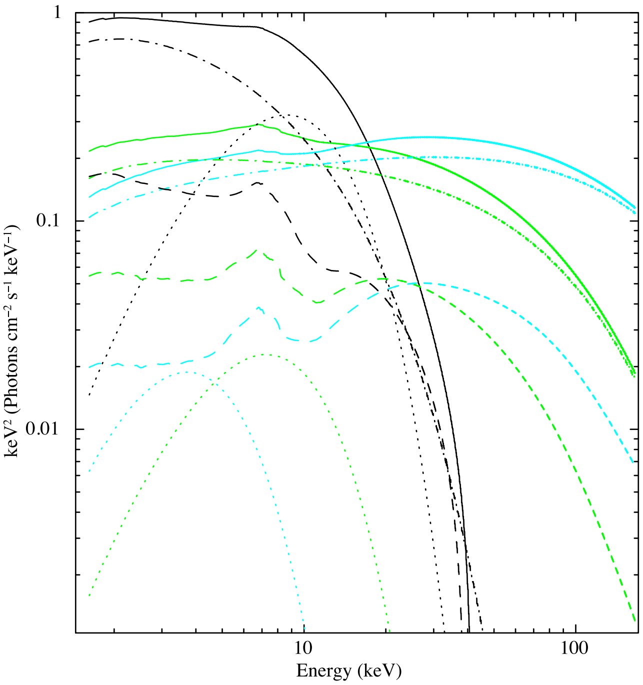

**Figure 8.** The unfolded best-fitting model CONST*PHABS*(BBODY+RELXILL) to the spectra of 4U 1636−53. The black, green and light blue lines correspond to each spectrum (only FPMA) listed from top to bottom in Table 1. The dot lines represent the BBODY component. The dash and dot–dashed lines represent the reflection and power-law spectra within the RELXILL model, respectively.

are larger than the corresponding ones in Model 2. The optical depth $\tau$ drops abruptly from Observations 1 to 2, then stays almost constant, but the values of the optical depth in Model 3 are smaller than those in Model 2. The high reflection fraction, $f_{\mathrm{refl}}$, indicates that reflection features in these spectra are important. We, therefore, plot the reflection and power-law components of Model 3 separately in Fig. 8. In order to show the reflected part clearly, we only plot the three unfolded model spectra of FPMA in Fig. 8. In the middle panel of Fig. 5, we show the $\Delta\chi^2$ of the fit versus the inclination for Model 3.

In order to investigate the ion geometry of 4U 1636−53, we fitted the spectra with another reflection model RELXILLLP (García et al. 2014; Dauser, García & Wilms 2016), which assumes that the corona is a point source located at a height above the accretion disc along the spin axis of the compact object. For these fits, RELXILLLP takes the place of RELXILL so that the model becomes CONST*PHABS*(BBODY+RELXILLLP), hereafter Model 4. Most of the parameters of RELXILLLP are the same as those in RELXILL but, instead of the inner and outer emissivity indices, RELXILLLP contains one more parameter, $h$, which is the height of the corona. We set all the common parameters of RELXILLLP to the values that we used in RELXILL: $a$ to 0.27 and $R_{\mathrm{out}}$ to 400 $R_{\mathrm{g}}$. We successfully modelled the spectra with a reasonable inclination $i_{\mathrm{relp}} \sim 56°$. The best-fitting parameters of Model 4 are presented in Table 5. Most of the parameters of Model 4 follow the same trend as those of Model 3. $R_{\mathrm{in}}$ and $\tau$ are smaller in Model 4 than in Model 3, but the normalization, $k_{\mathrm{relp}}$, is higher than $k_{\mathrm{rel}}$. The bottom panel of Fig. 5 shows the $\Delta\chi^2$ of the fit versus the inclination for Model 4.

**Table 5.** Best-fitting parameters of the *NuSTAR* spectra of 4U 1636−53 with Model 4.

| Component | | Model 4<br>Observation 1 | <br>Observation 2 | <br>Observation 3 |
|---|---|---|---|---|
| | constant | | $1.00^f/1.02 \pm 0.01$ | |
| BB | $kT_{\mathrm{bb}}$ (keV) | $2.13 \pm 0.01$ | $1.82 \pm 0.02$ | $0.93 \pm 0.02$ |
| | $k_{\mathrm{bb}}$ ($10^{-3}$) | $9.2 \pm 0.02$ | $0.6 \pm 0.01$ | $0.5 \pm 0.01$ |
| | $F_{\mathrm{bb}}$ ($10^{-11}$) | $71.3 \pm 0.07$ | $4.4 \pm 0.05$ | $2.0 \pm 0.03$ |
| | | $64.6 \pm 0.07$ | $4.4 \pm 0.05$ | $2.5 \pm 0.03$ |
| RELXILLLP | $i_{\mathrm{relp}}(°)$ | | $55.7 \pm 0.2$ | |
| | $h/R_{\mathrm{g}}$ | $2.3 \pm 0.2$ | $2.5 \pm 0.1$ | $2.8^{+0.1}_{-0.3}$ |
| | $R_{\mathrm{in}}/R_{\mathrm{g}}$ | $5.7 \pm 0.07$ | $10.3 \pm 0.04$ | $11.4 \pm 0.08$ |
| | $\Gamma_{\mathrm{relp}}$ | $2.19 \pm 0.01$ | $1.93 \pm 0.01$ | $1.76 \pm 0.01$ |
| | $E_{\mathrm{cut}}$ (keV) | $7.9 \pm 0.05$ | $61.5 \pm 0.6$ | $135.9 \pm 0.7$ |
| | $\tau$ | $4.9 \pm 0.04$ | $1.5 \pm 0.02$ | $0.9 \pm 0.01$ |
| | $log(\xi)$ | $4.4 \pm 0.03$ | $3.4 \pm 0.03$ | $3.1 \pm 0.06$ |
| | $k_{\mathrm{relp}}(10^{-3})$ | $289.9^{+332}_{-0.3}$ | $46.7 \pm 0.05$ | $21.3 \pm 0.03$ |
| | $F_{\mathrm{relp}}$ ($10^{-9}$) | $1.4 \pm 0.01$ | $1.1 \pm 0.01$ | $1.2 \pm 0.01$ |
| | | $1.4 \pm 0.01$ | $1.1 \pm 0.01$ | $1.2 \pm 0.01$ |
| | Total flux $F_{\mathrm{ttl}}$ ($10^{-9}$) | $2.12 \pm 0.01$ | $1.13 \pm 0.01$ | $1.17 \pm 0.01$ |
| | | $2.11 \pm 0.01$ | $1.12 \pm 0.01$ | $1.19 \pm 0.01$ |
| | $\chi^2_\upsilon$ (dof) | | 1.04(4636) | |

*Notes.* Units are the same as in Table 2. The inclination of the RELXILLLP component is linked across the three observations.

## 4 DISCUSSION

We analysed three *NuSTAR* observations of the NS LMXB 4U 1636−53 in different states and found prominent positive broad residuals around 5–10 keV in all *NuSTAR* spectra, which indicates possible emission reflected off an accretion disc. We applied four different models to fit the residuals in the spectra, which are: a simple symmetric model, GAUSSIAN, a relativistically broadened emission-line model, KYRLINE, and two models including relativistically smeared and ionized reflection off the accretion disc, RELXILL and RELXILLLP. All models fitted the data well, although KYRLINE and RELXILL yield an inclination of the accretion disc, ∼88°, which is at odds with the fact that no dips or eclipses have been observed in this source. The RELXILLLP model, however, gives a reasonable inclination of ∼56°. Additionally, the flux and the EW of the emission line are anti-correlated with the flux of the hard illuminating source in Model 2.

Previous work on modelling the reflection spectrum of 4U 1636−53 have found high inclination angles (e.g. Pandel et al. 2008; Sanna et al. 2013). By modelling three *XMM–Newton* spectra with the DISKLINE component, which describes relativistically broadened line emission from a disc around a non-rotating black hole, Pandel et al. (2008) reported that the inclination in all cases is larger than 64° and consistent with 90°. Sanna et al. (2013) analysed six *XMM–Newton* observations and found that most of them give high inclination values. Fitting the KYRLINE model to the *NuSTAR* data, as in the case of Sanna et al. (2013), we also found an inclination of ∼88°. In this case, contrary to the case of the *XMM–Newton* data, this cannot be due to pile-up or similar calibration issues.

We also modelled the data with two relativistically blurred reflection models, RELXILL and RELXILLLP. Compared with angle-averaged reflection models of the line, RELXILL and RELXILLLP calculate the reflection fraction, relativistic blurring and angle-dependent reflection spectrum for different coronal heights self consistently. The best-fitting inclination angle in RELXILL is still higher than 80°, similar to that in KYRLINE. Ludlam et al. (2017) applied the same RELXILL

Downloaded from https://academic.oup.com/mnras/article-abstract/468/2/2256/3073721 by guest on 20 July 2020

model to one *NuSTAR* observation taken before our observations and they also obtained a high inclination of 76.5°–79.9°. The best-fitting inclination angle is reasonable in RELXILLLP, ∼56°. RELXILLLP assumes a lamp post geometry of the primary source of the illuminating hard X-rays. In black hole systems, the reflection fraction in RELXILLLP describes how much flux is emitted towards the disc compared to how much is emitted directly to the observer. Therefore, the fraction of photons hitting the accretion disc can be directly measured, making it possible to set constraints on the geometry of the system. The RELXILL model does not assume any geometry and does not take any relativistic boosting effects into account (Dauser et al. 2016). A further exploration of the reason why RELXILLLP gives a more reasonable inclination angle is beyond the scope of this work.

Using RELXILLLP, we found that the primary source is located close to the NS, at a height of $h \sim 2$–$3\ R_{\rm g}$, which is consistent with the fact that in similar accreting systems (black holes and AGNs, e.g. Dauser et al. 2013; Fabian et al. 2014) the corona is compact. Alternatively, in an NS system, the small height could also refer to the boundary layer between the accretion disc and the NS surface as the primary source of the illuminating hard X-rays (see Sanna et al. 2013). Additionally, different from other sources (e.g. Parker et al. 2014; Ludlam et al. 2016), the iron emission line that dominates the emission at 5–10 keV of the reflection spectra of 4U 1636−53 is stronger than the Compton hump that dominates the emission at above 10 keV, especially in Observation 1 (see Fig. 8). Dauser et al. (2014) suggested that high spin sources produce strong relativistic reflection features. They gave the maximum possible reflection fraction as a function of spin in fig. 3 of their paper. Based on the frequency of 4U 1636−53, we fixed the spin at 0.27 in this work (see Section 3.1). As for a spin of 0.27, the corresponding maximum reflection fraction is ∼1.2 in Dauser et al. (2014), which is consistent with our reflection fraction values in Table 4.

In REXILL/LP, the illuminating source is assumed to be a corona, which is described as a power law with a high-energy cut-off. Given this assumption in REXILL/LP, the corona is responsible for the main contribution of the reflected spectra in Observations 2 and 3. As for Observation 1, 4U 1636−53 is likely in the soft state and the corresponding $E_{\rm cut}$ is around 7–8 keV. The low value of the $E_{\rm cut}$ indicates that the illuminating source that produces the reflection component in Observation 1 may not be the corona. Sanna et al. (2013) reported that in two out of six observations (Observations 2 and 6 in their work), the illuminating source is essentially the corona, whereas in the other four observations, the main illuminating source is the surface/boundary layer. Observation 2 in their work is also in the soft state and the cut-off energy of the component that represented the corona was $E_{\rm cut} = 9.5^{+0.9}_{-0.8}$ keV. Therefore, we cannot conclude whether the primary source in Observation 1 is the corona or the NS surface/boundary layer, only based on the low value of the cut-off energy.

In most cases, the temperature of the BBODY component is higher than 1 keV in LMXBs (e.g. Cackett et al. 2010; Ng et al. 2010; Lyu et al. 2014). However, the $kT_{\rm bb}$ in Observation 3 is always below 1 keV in all of our models. In order to test whether this is due to the lack of a DISKBB component, we added a DISKBB component in our model, even if it is not required by the data (see Sanna et al. 2013). Given the lack of data below 3 keV, we cannot constrain $kT_{\rm dbb}$. We therefore assumed an average temperature of 0.5 keV (Sanna et al. 2013), and fixed it in all observations; we set the normalization free to vary but linked them within each observation. For instance in Model 1, $kT_{\rm bb}$ increased to $1.92 \pm 0.10$, $1.50 \pm 0.03$ and $1.06 \pm 0.08$ keV in Observation 1, 2 and 3, respectively. As we suspected, the temperature of the BBODY component is affected by the presence/absence of a disc component. Especially in the hard state, $kT_{\rm dbb}$ can be very low, around ∼0.2 keV (Sanna et al. 2013), therefore, the BBODY component shifts to lower temperatures to compensate for the emission of the accretion disc. This may be the reason why the $kT_{\rm bb}$ in Observation 3 is so low. Actually, the absence of a DISKBB component in Model 1 affects not only the BBODY component, but also the GAUSSIAN component. As we mentioned in Section 3, if we allowed the energy of the line in the GAUSSIAN component to be below 6.4 keV, the energy of the line in Observation 2 and 3 decreases, especially in Observation 3. Using the command *steppar* in XSPEC, we found that when we fit the line with a GAUSSIAN, the energy of the line is correlated with the $kT_{\rm bb}$ in Observation 3. On the contrary, there is no correlation between the energy of the line in the KYRLINE component and the $kT_{\rm bb}$ in Model 2. These results indicate that the GAUSSIAN component in Model 1 is very sensitive to the lack of a DISKBB component.

Shih et al. (2005) reported a ∼40 d period in the *RXTE*/ASM light curve of 4U 1636−53, which they interpret as accretion rate variability due to the X-ray irradiation of the disc. As the X-ray luminosity decreases, the accretion disc is not fully ionized. As a consequence, the outer regions of the disc cool down, and thereby the overall mass accretion decreases, subsequently leading to an X-ray minimum. The inner edge of the disc recedes as a result of the mass accretion reducing in the inner regions because the high-density disc material there will be exhausted and likely be replaced by a hot corona. The three *NuSTAR* observations analysed here were taken over a few days covering more or less the full ∼40 d period. The evolution of our spectral parameters supports the interpretation of Shih et al. (2005). The photon index, Γ, in all models decreases and the cut-off energy, $E_{\rm cut}$, increases from Observations 1 to 3, which indicates that the system evolves from the soft, to the transitional, and finally to the hard state (see Sanna et al. 2013). The BBODY component weakens dramatically from Observations 1 to 3 (e.g. Lyu et al. 2014), which matches the picture above. In principle, the parameters of the BBODY component do not have a clear correlation with the source state. However, keeping in mind the possibility that the BBODY component is partly fitting the emission of the DISKBB component, the temperature of the BBODY component decreases from Observations 1 to 3, probably due to a drop of the temperature of the DISKBB component. Besides that, the reflection continuum also shows a strong correlation with the source state. According to the standard accretion disc model, as mass accretion rate decreases, the disc moves outwards (e.g. Esin, McClintock & Narayan 1997). The inner disc radius, both in RELXILL and RELXILLLP, increases from Observations 1 to 3. As the mass accretion rate decreases, the disc becomes less ionized, resulting in the $\xi$ and the energy of the line, $E_{\rm gau}$ and $E_{\rm kyr}$, dropping.

We also found that the flux and the EW of the emission line when fitted with the model KYRLINE is anti-correlated with the flux of the NTHCOMP component in Model 2. Lyu et al. (2014) found that the flux and the EW of the iron line first increase and then decrease as the flux of the Comptonized component increases when the flux of the Comptonized component is higher than $15 \times 10^{-10}\,{\rm erg\,cm^{-2}\,s^{-1}}$. All the fluxes of the KYRLINE in Model 2 fall into this region of the plot. Lyu et al. (2014) explained this anti-correlation either by gravitational light bending of the primary source, or by changes in the ionization states of the accretion disc. In the light bending model (Miniutti & Fabian 2004), the reflection fraction is correlated to the height of the primary source above the disc. When the source height is small, within a few $R_{\rm g}$ of the disc, relativistic light bending results in a small fraction of the emitted photons escaping to

Downloaded from https://academic.oup.com/mnras/article-abstract/468/2/2256/3073721 by guest on 20 July 2020

infinity and a large fraction of the emitted photons bent towards the disc. The height, *h*, of the corona in Model 4 supports this idea as well.

## 5 CONCLUSIONS

We modelled the spectra of three *NuSTAR* observations of the source 4U1636−53 in different states. Four models fitted all spectra equally well but with different line profiles. Even though the simplest symmetric GAUSSIAN fitted the data well, the breadth of the line, $\sigma > 1.22$ keV, is unlikely to be produced only by Compton broadening. Both the phenomenological model KYRLINE and the reflection model RELXILL gave an unrealistically high inclination of the accretion disc. Given that this is the first report on the reflection spectrum of *NuSTAR* data of 4U1636−53, the high inclination from KYRLINE at least excludes the possible effect of calibration uncertainties of the *XMM–Newton* data which yielded a similarly high inclination (see Sanna et al. 2013). We find a reasonable inclination from the lamp post reflection model RELXILLLP. In addition, we provide a possible explanation as to why the temperature of BBODY is lower than 1 keV in this work. We also explored the variation of the direct and reflection continuum as a function of the source state. We find and confirm that most of the spectral parameters in 4U 1636−53 are strongly correlated with the source state.

## ACKNOWLEDGEMENTS

We thank the referee for many invaluable comments and suggestions. We also thank, Thomas Dauser, for the kind explanation of their models, RELXILL and RELXILLLP. DA acknowledges support from the Royal Society. TMB acknowledges financial contribution from the agreement ASI-INAF I/037/12/0. This research is based on the data from the *NuSTAR* mission, a project led by the California Institute of Technology, managed by the Jet Propulsion Laboratory and funded by NASA. This work has made use of data from the High Energy Astrophysics Science Archive Research Center (HEASARC), provided by NASA/Goddard Space Flight Center (GSFC).

## REFERENCES

Altamirano D., van der Klis M., Méndez M., Jonker P. G., Klein-Wolt M., Lewin W. H. G., 2008, ApJ, 685, 436
Belloni T., Homan J., Motta S., Ratti E., Méndez M., 2007, MNRAS, 379, 247
Braje T. M., Romani R. W., Rauch K. P., 2000, ApJ, 531, 447
Cackett E. M. et al., 2008, ApJ, 674, 415
Cackett E. M. et al., 2010, ApJ, 720, 205
Dauser T., Garcia J., Wilms J., Böck M., Brenneman L. W., Falanga M., Fukumura K., Reynolds C. S., 2013, MNRAS, 430, 1694
Dauser T., García J., Parker M. L., Fabian A. C., Wilms J., 2014, MNRAS, 444, L100
Dauser T., García J., Wilms J., 2016, Astron. Nachr., 337, 362
Dauser T., García J., Walton D. J., Eikmann W., Kallman T., McClintock J., Wilms J., 2016, A&A, 590, A76
Dovčiak M., Karas V., Yaqoob T., 2004, ApJS, 153, 205
Esin A. A., McClintock J. E., Narayan R., 1997, ApJ, 489, 865
Fabian A. C., Rees M. J., Stella L., White N. E., 1989, MNRAS, 238, 729
Fabian A. C., Parker M. L., Wilkins D. R., Miller J. M., Kara E., Reynolds C. S., Dauser T., 2014, MNRAS, 439, 2307
Galloway D. K., Psaltis D., Muno M. P., Chakrabarty D., 2006, ApJ, 639, 1033
García J. et al., 2014, ApJ, 782, 76
García J. A., Dauser T., Steiner J. F., McClintock J. E., Keck M. L., Wilms J., 2015, ApJ, 808, L37
Giles A. B., Hill K. M., Strohmayer T. E., Cummings N., 2002, ApJ, 568, 279
Guilbert P. W., Rees M. J., 1988, MNRAS, 233, 475
Harrison F. A. et al., 2013, ApJ, 770, 103
Hasinger G., van der Klis M., 1989, A&A, 225, 79
Lightman A. P., White T. R., 1988, ApJ, 335, 57
Ludlam R. et al., 2016, ApJ, 824, 37
Ludlam R. M. et al., 2017, ApJ, 836, 140
Lyu M., Méndez M., Sanna A., Homan J., Belloni T., Hiemstra B., 2014, MNRAS, 440, 1165
Miller M. C., Lamb F. K., Cook G. B., 1998, ApJ, 509, 793
Miller J. M. et al., 2013, ApJ, 775, L45
Miniutti G., Fabian A. C., 2004, MNRAS, 349, 1435
Mitsuda K. et al., 1984, PASJ, 36, 741
Ng C., Díaz Trigo M., Cadolle Bel M., Migliari S., 2010, A&A, 522, A96
Pandel D., Kaaret P., Corbel S., 2008, ApJ, 688, 1288
Parker M. L. et al., 2014, MNRAS, 443, 1723
Popham R., Sunyaev R., 2001, ApJ, 547, 355
Risaliti G. et al., 2013, Nature, 494, 449
Sanna A., Hiemstra B., Méndez M., Altamirano D., Belloni T., Linares M., 2013, MNRAS, 432, 1144
Sanna A., Méndez M., Altamirano D., Belloni T., Hiemstra B., Linares M., 2014, MNRAS, 440, 3275
Shih I. C., Bird A. J., Charles P. A., Cornelisse R., Tiramani D., 2005, MNRAS, 361, 602
Strohmayer T. E., Markwardt C. B., 2002, ApJ, 577, 337
Sunyaev R. A., Titarchuk L. G., 1980, A&A, 86, 121
van Paradijs J. et al., 1990, A&A, 234, 181
Zdziarski A. A., Johnson W. N., Magdziarz P., 1996, MNRAS, 283, 193
Zhang W., Lapidus I., Swank J. H., White N. E., Titarchuk L., 1997, IAU Circ., 6541
Zhang G., Méndez M., Sanna A., Ribeiro E. M., Gelfand J. D., 2017, MNRAS, 465, 5003
Życki P. T., Done C., Smith D. A., 1999, MNRAS, 309, 561

This paper has been typeset from a TEX/LATEX file prepared by the author.

Downloaded from https://academic.oup.com/mnras/article-abstract/468/2/2256/3073721 by guest on 20 July 2020